Final Report:

A multi-surface plasticity model for 3D wave propagation simulation using AWP

(SCEC Project 17162)

November 12, 2018

Investigators:

Daniel Roten[1] (PI)
Kim Olsen[1] (co-PI)
Yifeng Cui[2] (co-PI)

Institutional Affiliations:

1. San Diego State University
   Dept. Geological Sciences
   5500 Campanile Dr, MC 1020
   San Diego, CA 92182-1020

2. University of California San Diego
   San Diego Supercomputer Center
   9500 Gilman Dr, MC 0505
   La Jolla, CA 92093-0505

Abstract

We have implemented an Iwan-type plasticity model in the CPU version of the AWP finite difference (FD) code. AWP-Iwan tracks a series of von Mises yield surfaces arranged in a parallel-series configuration, which in combination reproduce Masing unloading and reloading behavior in three dimensions. The implementation was verified against the 1D FD difference code Noah by simulating the site response of the KiK-net site KSRH10. A verification run for a 2D sediment-filled valley was also carried out, using solutions obtained with Noah2D as a reference. Synthetics obtained with AWP-Iwan using 20 yield surfaces were found to be consistent with the reference solutions in the time and frequency domains. AWP-Iwan was deployed on NCSA Blue Waters to simulate a M 7.8 earthquake on the southern San Andreas fault with realistic near-surface nonlinear behavior in the fill of sedimentary basins. These simulations confirm the importance of nonlinear effects on long-period surface waves during a ShakeOut-type earthquake scenario, with spectral accelerations at 3s reduced by $\sim$50% in Whittier Narrows and downtown Los Angeles with respect to a linear simulation.

Introduction

Simulations of the ShakeOut scenario, which assumes a southeast-northwest rupturing M 7.8 earthquake on the southern San Andreas fault (SAF) (e.g., Olsen *et al.*, 2006; Graves *et al.*, 2008; Olsen *et al.*, 2009; Bielak *et al.*, 2010), have shown that the string of contiguous sedimentary basins between the Southern San Andreas fault (SAF) and the Los Angeles basin (LAB) would act as a waveguide and channel long-period surface waves into densely populated urban areas. The presence of this waveguide effect has also been confirmed from independent observations in the form of virtual earthquakes (Denolle *et al.*, 2013), which were constructed from Green's functions derived from the ambient seismic field.

However, subsequent simulations of the M 7.8 ShakeOut scenario for a nonlinear medium predicted long-period ($>$1 s) shaking levels which were 30–70% lower in the LAB than the corresponding linear solutions (Roten *et al.*, 2014). These reductions were caused by both nonlinear attenuation of long-period surface waves (e.g., Joyner, 2000; Sleep, 2010; Sleep and Erickson, 2014; Sleep, 2014) and fault zone plasticity effects (e.g., Andrews, 2005; Ma, 2008; Duan and Day, 2010; Harris *et al.*, 2011). Recent high-resolution simulations of a M 7.7 earthquake on a slightly shorter segment of the SAF found even stronger nonlinear effects (Roten *et al.*, 2016) at higher frequencies (2 Hz), and concluded that nonlinearity must be included to bring simulated near-fault accelerations in line with ground motion prediction equations. Accounting for nonlinear material response, both in the fault zone and in soft sediments near the surface, will be imperative if physics-based ground motion predictions are to be performed at frequencies above 1 Hz.

A limitation of our previous nonlinear 3D simulations arises from the use of a relatively simple Drucker-Prager (DP) yield condition (equivalent to the Mohr-Coulomb model in 1D). In this model, the stress-strain relationship remains linear until the yield stress is reached (Fig. 1a). However, laboratory experiments performed on soils and soft rocks indicate a gradual reduction of the shear modulus (e.g., Hardin and Drnevich, 1972) and a reduction in the slope of the stress-strain curve (Fig. 1b) with increasing strain.

Because the energy dissipated per cycle (proportional to the area within the hysteresis loop) is larger in the DP model than in the more realistic hyperbolic model (Fig. 1), wave propagation simulations with a DP yield condition may overestimate the amount of damping in soils and rocks, and therefore result in ground motion predictions that are too low. On the other hand, a perfectly elasto-plastic yield model neglects the observed departure from linear behavior at low strains levels in soils, which would lead to overpredictions of ground motions.

In the framework of a previous SCEC-funded proposal (16264), we investigated the accuracy of the DP yield condition in modeling the nonlinear attenuation of long-period surface waves. We simulated the propagation of P-SV waves waves in two dimensions along a cross-section connecting the southern SAF with the LAB using both a 2D version of AWP and the Noah2D code (Bonilla *et al.*, 2006; Gélis and Bonilla, 2012, 2014) for a maximum frequency of 1 Hz. These simulations showed that the hyperbolic soil model implemented in Noah2D result in lower ground motions than the simple Drucker-Prager yield condition.

The scope of SCEC project 17162 was to add support for a more sophisticated soil model in AWP, which will track laboratory observations of shear modulus degradation in soils and soft rocks.

Iwan Model in Three Dimensions

The idea behind the Iwan model is that a material governed by hysteretic behavior can be thought of as a large number of elastic, perfectly-plastic components having different yield levels. In the 1D (uniaxial) case, this can be illustrated using an assembly of elastic springs and plastic sliders, which can either be arranged in a series-parallel or parallel-series (Fig. 2a) configuration. Each single spring-slider combination obeys an ideal elastoplastic stress-strain relationship as shown in Figure 1a. Iwan (1967) and Mroz (1967) showed that the combined system of spring-slider elements follows a hyperbolic path as given in Figure 1b, in agreement with the Masing (1926) criteria which are frequently used to describe the behavior of soils under cyclic loading (e.g., Kramer, 1996). Although Iwan (1967) focused on the series-parallel model to extend this approach to 3D, later studies on multi-axial cyclic plasticity (Chiang, 1992; Chiang and Beck, 1994; Einav, 2005; Einav and Collins, 2008) demonstrated that a much simpler 3D model can be developed based on the parallel-series model. In this approach, the yield surfaces of individual components remain fixed, eliminating the need for moving the nested yield surfaces and preventing them from overlapping. Therefore, we chose the parallel-series model for implementation in AWP.

Implementation of Iwan model in AWP

A prototype of the AWP-CPU code which support multiple yield surfaces has been developed and tested. The code tracks a series of von Mises yield surfaces arranged in a parallel-series configuration, which in combination reproduce Masing (1926) unloading-and reloading behavior as well as the Bauschinger effect, using a modeling approach also known as overlay concept (Kaklamanos *et al.*, 2015). Because the AWP-Iwan prototype tracks the stress tensor pertaining to every yield surface, the implementation required extensive changes to the code. While the six independent components of the stress tensor were previously stored in 3D arrays reflecting the 3D geometry of the medium, AWP-Iwan used 4D arrays, where the 4th dimension reflects the number of the element associated with the stress tensor. 4D arrays are also required for the two

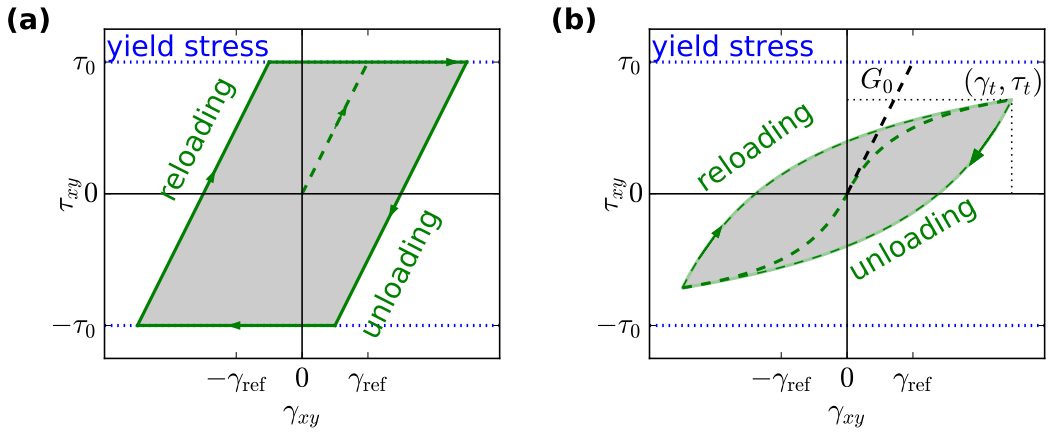

Figure 1: Stress-strain loops in simple shear described using *(a)* Mohr-Coulomb and *(b)* hyperbolic soil models. γ_{xy} = shear strain, τ_{xy} = shear stress, γ_{ref} = reference strain, τ_0 = yield stress, G_0 = low strain shear modulus (modified from Bonilla, 2001).

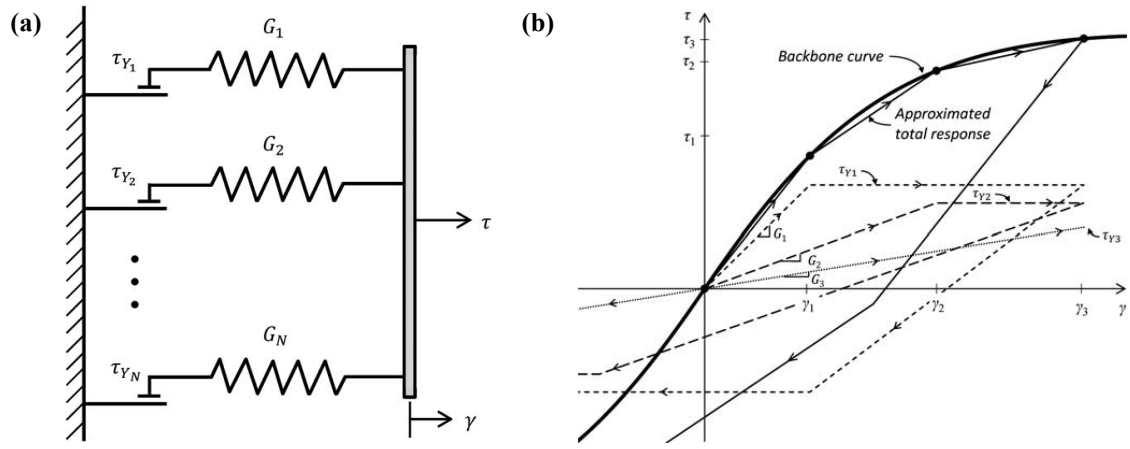

Figure 2: *(a)* Schematic representation of 1D parallel-series Iwan model and *(b)* stress-strain behavior of 3 elastoplastic elements in parallel (from Kaklamanos *et al.*, 2015).

Lame parameters λ and μ and the yield stress $\tau_{\max}$, which are computed for each yield surface following Kaklamanos *et al.* (2015). AWP-CPU uses the message passing interface (MPI) and geological domain decomposition to distribute the computational cost over several nodes (Cui *et al.*, 2010), and both stresses and velocities within a two-layer ghost cell regions are exchanged with adjacent subdomains after each stress and velocity update. Because the stress tensors are represented by 4D arrays in the AWP-Iwan prototype, the stress exchange subroutines were also subject to major modifications during the implementation of the advanced nonlinear model. Velocity vectors and densities, on the other hand, are still stored in 3D arrays, and velocity updates are computed from the compound (overlay) stress field which is obtained by summation over the individual stress tensors. Figure 3 compares a reference backbone and shear modulus reduction curve (computed for a reference strain of $\gamma_r = 10^{-3}$) with the values approximated by 7 yield surfaces.

Support for the Iwan model was also included in the subroutines for simulation of dynamic rupture in AWP-CPU. In dynamic rupture mode, the code allocates additional stress arrays for the zone surrounding the fault, which were expanded to 4D as well. Because the ghost cell regions of these fault zone stress arrays are swapped with adjacent subdomains during each iteration, stress exchange subroutines pertaining to dynamic rupture also had to be adjusted to accommodate these expanded stress arrays.

Verification against Noah code

To verify that AWP-Iwan produces accurate results, we applied the method to previously studied 1D and 2D problems, and compared synthetics against reference solutions. The Noah program (Bonilla *et al.*, 2005, 2006) is well suited to compute reference solutions, because it has been verified against many other nonlinear codes and validated against observations within the PRENOLIN project (Régnier *et al.*, 2018). Running these tests depended on new features for the treatment of boundary conditions and the incoming wavefield which were implemented in AWP.

Periodic boundary conditions in AWP

In order to effectively simulate the response of the selected KiK-net sites KSRH10 to an incoming plane wave, the option to use periodic boundary conditions at the lateral edges of the domain was added in both the CPU and GPU version of the AWP code. The use of periodic boundary conditions allows such 1D simulations to be carried out using a smaller domain size, which saves computational time. In addition, if the medium

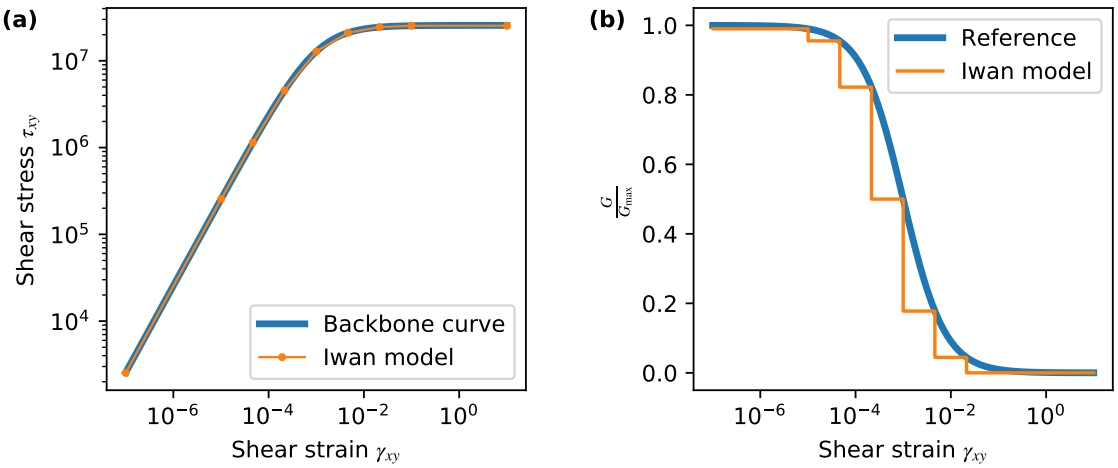

Figure 3: *(a)* Backbone curve showing shear stress as function of shear strain for a hyperbolic model with a reference strain of $\gamma_r = 10^{-3}$ (blue) and the Iwan model using 7 spring-slider combinations (orange). *(b)* Shear modulus reduction curve in the reference solution and approximated by the Iwan model.

is laterally homogeneous and the input wave field consists only of vertically propagating body waves (plane strain conditions), the AWP code can be used to model site response in 1D. Results computed in such plane strain simulations can be compared directly against solutions obtained from well established 1D propagators.

Plane wave input in AWP

We also added a new option for defining the seismic source in the AWP code. While it was previously only possible to define either kinematic or dynamic (in case of AWP-CPU) finite sources and point sources located within the domain, the code now optionally accepts a recorded ground motion which is imposed as incoming plane wave at the bottom of the computational domain. This feature is necessary for performing site response simulations in AWP, which are carried out for code verification and validation problems.

Verification for 1D case

We performed a 1D simulation of vertical wave propagation using the velocity structure at the KiK-net site KSRH10, which was used as one of the two test sites in the PRENOLIN project (Régnier *et al.*, 2018). The downhole E-W seismogram of a M 6 earthquake recorded on November 29, 2004 was used as input signal. The simulation was carried out using AWP for a viscoelastic linear medium and a nonlinear medium represented by 20 yield surfaces (Fig. 4). We computed reference solutions using the Noah (Bonilla *et al.*, 2005) code for the linear case and the nonlinear case using the strain space multishear plasticity model (Iai *et al.*, 1992). We used a grid spacing of $\Delta h = 2$ m for AWP and $\Delta h = 1$ m for Noah, as AWP is 4th order accurate in space, while Noah uses a 2nd order finite difference operator. We use the reference strain γ_r to control the strength of soils in both AWP and Noah. We derived the reference strain from the shear strength $\tau_{\max}$, which was computed from friction angles and cohesion provided for the site KSRH10 in Régnier *et al.* (2015). P-and S-wave velocities, densities and quality factors were also adopted from Régnier *et al.* (2015). As expected, solutions are virtually identical in the linear case (Fig. 4). Time series obtained with AWP-Iwan closely follow the reference solution obtained with Noah using the generalized Masing rules (Fig. 4). As already noted by Kaklamanos *et al.* (2015), we found that using 10–15 yield surfaces produces acceptable results, although the accuracy of the solution decreases with decreasing number of yield surfaces. Surface-to-

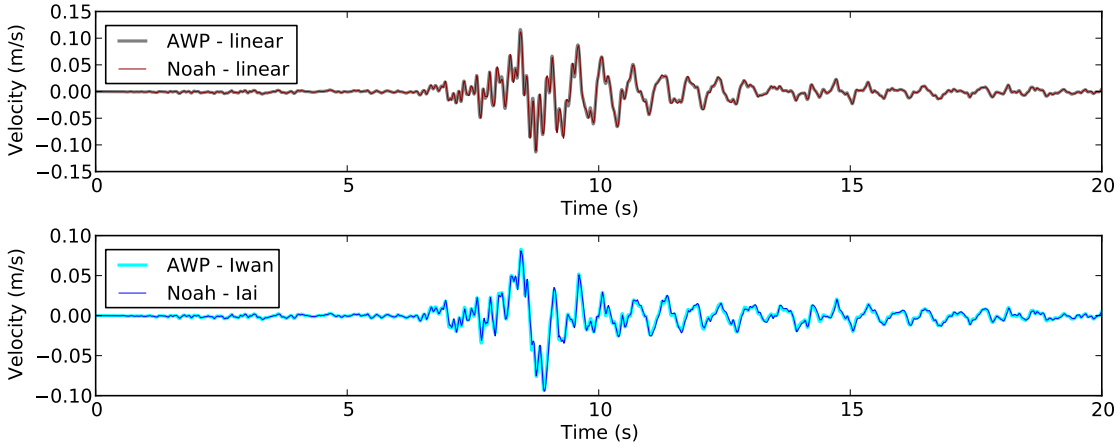

Figure 4: Comparison of simulated surface velocity time series at KiK-net site KSRH10 obtained with AWP and Noah in *(a)* linear (viscoelastic) and *(b)* nonlinear case using the Iwan model and the strain-space-multishear model (Iai *et al.*, 1992), respectively.

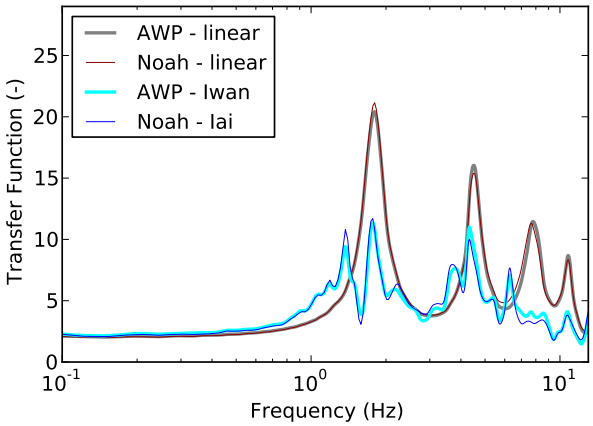

Figure 5: Surface-to-borehole Fourier transfer functions at KSRH10 obtained using AWP and Noah.

borehole transfer functions (Fig. 5) obtained with AWP-Iwan are also consistent with the reference solutions, predicting a similar reduction in amplitude and shift of resonance frequencies.

Verification for 2D case

To analyze the performance of AWP-Iwan in the presence of lateral heterogeneities, we carried out a 2D simulation of P-SV wave propagation for a generic sediment-filled valley. We specified the sediment-bedrock interface as a constant slope on the left side and sine-shaped on the right side (Fig. 6b). We defined a shear-wave velocity of 3,200 m/s in bedrock and 200 m/s at the surface of the basin, resulting in a high velocity contrast. Sediments within the basin are layered horizontally, and velocities and densities are constant inside each layer. The shear wave-velocity reaches 750 m/s in the lowermost layer. We specified a reference strain of γ_r=10^{-3} in the uppermost layer, $\gamma_r = 5{\cdot}10^{-3}$ in the second layer (50-100 m depth) and $\gamma_r = 10^{-2}$ in the third layer (100 - 200 m depth). The basin was excited using a vertically propagating, planar shear-wave with

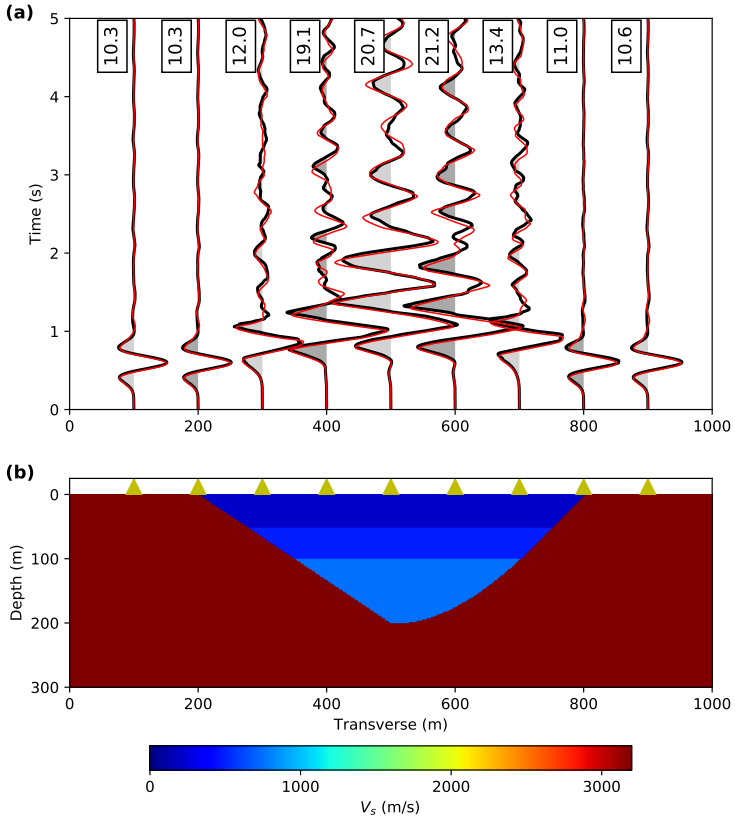

Figure 6: *(a)* Comparison of transverse velocity time series obtained from 2D nonlinear P-SV wave propagation inside a sediment-filled valley. Black semi-filled wiggles show the solution obtained with AWP-Iwan; the reference solution calculated by Noah2D is plotted in red. *(b)* Cross-section through valley with shear-velocity and location of plotted stations.

the transverse (perpendicular to the valley axis) particle motion. A Ricker wavelet with a center frequency of 3 Hz was used as source time function. Unfortunately, the implementation of viscoelastic attenuation in Noah2D results in numerical instabilities near the strong lateral velocity contrasts at the basin edges (Fabian Bonilla, written communication, 2018). Therefore, the verification for the 2D case was performed without viscoelastic attenuation. We note that no instabilities with the Q implementation were recorded in AWP-Iwan for linear or nonlinear computations.

Figure 6a compares ground motions in the transverse direction obtained with AWP and Noah2D in the nonlinear case. Time series obtained with AWP and Noah are very similar in shape and amplitude. In both codes, peak velocities in the valley center are reduced from 38 cm/s in the linear case (not shown) to 20 cm/s in the nonlinear case; in addition, the nonlinearity greatly reduces the duration of the shaking, and this feature is also reproduced well by AWP-Iwan.

These results imply that the Iwan model works as expected in the AWP code. Due to the lack of available 3D nonlinear wave propagation codes and benchmarks, no verification of AWP-Iwan in the 3D case has been performed so far. Verification of nonlinear codes for 3D benchmarks is currently planned as part of a collaborative SCEC proposal within the Technical Activity Group (TAG) on nonlinearity in the shallow crust.

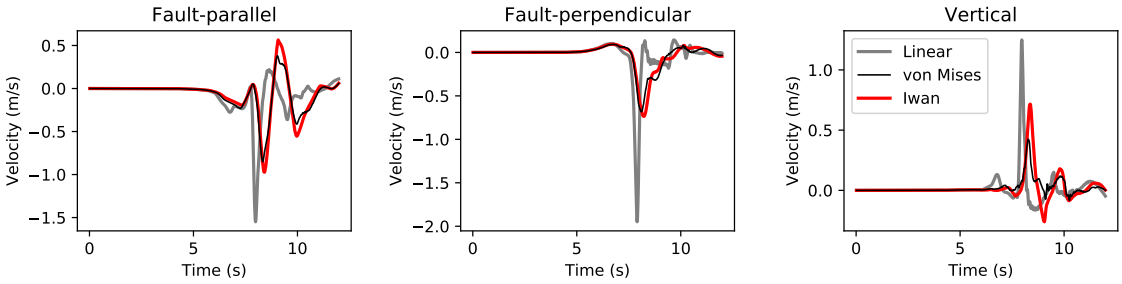

Figure 7: Simulated surface ground motions on top of the fault for SCEC dynamic rupture code verification benchmark TPV26/27 using a linear medium, a single von Mises yield surface, and Iwan model using 10 yield surfaces.

Test of AWP-Iwan for dynamic rupture

To ascertain that the Iwan model produces reasonable results in dynamic rupture mode, we performed the SCEC code verification benchmark exercise TPV26/TPV27 using both the traditional version of AWP and AWP-Iwan. We computed a reference solution using a linear medium (TPV26) and a nonlinear medium using a single yield surface (TPV27). We note that although we used a pressure-independent von Mises yield surface for the nonlinear solution, as opposed to a pressure dependent Drucker-Prager yield surface, pressure dependence was included by defining the failure stress from the initial stress, friction angle and cohesion prescribed in the benchmark description. For the Iwan model we used 10 von Mises yield surfaces. Solutions obtained with the Iwan model are similar to the reference solution obtained with a single von Mises yield surface, with significantly reduced peak velocities compared to the linear solution (Fig. 7). Because the stress-strain relationship in the Iwan model is very different from a purely elasto-plastic, single von Mises or Drucker-Prager yield surface, the solutions are not expected to be identical.

Simulation of the M 7.8 ShakeOut scenario using Iwan model

We deployed AWP-Iwan on NCSA Blue Waters to explore how realistic nonlinear surface attenuation would affect long-period ground motions during a future large earthquake on the southern San Andreas fault. We adopted the dynamic rupture model of Roten *et al.* (2017), which defines a high stress-drop earthquake rupturing a 250 km planar fault segment from Indio to Lake Hughes from southeast to northwest. This possible outcome for a future M 7.8 San Andreas earthquake event is also known as the ShakeOut scenario (Jones *et al.*, 2008).

Definition of nonlinear parameters

We used the EPRI93 shear modulus reduction curves for Sand (Electric Power Research Institute, 1993) to define depth-dependent reference strains inside the sedimentary fill of basins, which were identified as regions where $v_s < 1{,}950$ m/s. The reference strain γ_r assigned inside basins ranges from 0.1% near the surface to 0.5% at depths of 300 m or more. Outside basins, a value of $\gamma_r = 2\%$ for rock was assigned (Schnabel *et al.*, 1972). At depths of 6 km or more, we set a reference strain of 100%, effectively prohibiting nonlinearity.

Definition of initial stress

In nonlinear wave propagation simulations, the absolute value of the initial stress also needs to be defined. For regions inside rock we followed the initial stress definition used in a previous study (Roten *et al.*, 2017),

and assumed that the major principal stress, σ_1 is rotated by 45° with respect to the fault, with a ratio of $\sigma_1 = 1.4\ \sigma_2$ and $\sigma_2 = 0.6\ \sigma_3$. between principal stresses. The intermediate principal stress, σ_2, was taken as vertical and computed from the lithostatic load. Inside sedimentary basins, we assumed hydrostatic stress conditions, with $\sigma_1 = \sigma_2 = \sigma_3$.

Initial stress loading in Iwan model

A further complication with initial stresses arises from the hysteretic stress-strain relationship in the Iwan model, because the position in stress-strain space is not uniquely defined by the initial stress (i.e., the strain can not be inferred from the stress). A few of the weaker sliders in the spring-slider assembly typically reach their yield value if the configuration is loaded to realistic initial stress. Here, we define the initial state of the individual stress tensors using an iterative procedure, where the initial stress is first distributed over the different spring-slider elements proportionally to their shear moduli (spring constant). If the resulting stress is below the target value due to yielding of one or more elements, the residual stress is distributed over the remaining (non-yielding) spring-slider elements, and the procedure is repeated until the target stress is reached.

For the ShakeOut simulations using the Iwan model, initial loading was performed to 1.5 times the target stress (50% overshoot), and each springs was subsequently relaxed proportionally to its strength to reach the target stress. This approach avoids initial stress tensors touching their yield surface at the beginning of the simulation, and reflects loading and subsequent unloading of the medium during previous events.

Ground motion results

Figure 8 compares spectral accelerations at 3s (3s-SAs) obtained in a linear simulation with values derived from the nonlinear simulation using the Iwan model. Shallow soil nonlinearity reduces ground motions especially along the waveguide connecting the SAF with the LAB. 3s-SAs are reduced by ∼50% at sites rus (Whittier Narrows) and dla (downtown Los Angeles). Figure 9 compares simulated waveforms at the sites clt (Colton), rus and dlu obtained from the two simulations, along with results obtained from a Drucker-Prager yield condition using the Hoek-Brown failure criterion for a moderately fractured sandstone (Roten *et al.*, 2017). Hystereric damping in the Iwan model results in reduced peak ground velocities and suppression of reverberating surface waves with respect to a linear simulation, and both effects are more pronounced in the multi-surface Iwan model than in the single yield surface Drucker-Prager model.

AWP-Iwan keeps track of the minimum shear modulus (defined as the sum of the shear modulus associated with all non-yielding elements) encountered at each node during the simulation. Figure 10 shows the minimum value of the shear modulus G, normalized by the low-strain shear modulus G_{max}, at the surface of the domain. (Note that the value of G/G_{max} can only assume a few different values due to the limited number of yield surfaces.) The shear modulus is being reduced by ∼75% where the SAF intersects the low-velocity sediments of the San Bernardino basin, and reaches values close to zero (i.e., all elements are yielding) in a few localized areas. A ∼30 km long stretch with a G/G_{max} value of 50% marks the main waveguide along the Whittier-Narrows corridor, which connects the San Gabriel basin with the LAB. As simulations were carried out using a grid spacing of Δh = 100 m and minimum shear-wave velocity of 500 m/s, only frequencies up to 1 Hz can be resolved in the linear case. Because the shear modulus degradation reduces the effective shear-wave velocity, the frequency limit will be reduced in the simulations with the Iwan model. For example, if the shear-modulus is reduced to 25% of G_{max}, the shear wave velocity $v_s = \sqrt{G/\rho}$ is reduced to 50%, and the frequency limit is reduced to 0.5 Hz. To account for this effect, it is customary to increase the minimum number of points per wavelength *a priori* (e.g. Bonilla *et al.*, 2005), because the effective shear modulus reduction is only known after the simulation is completed.

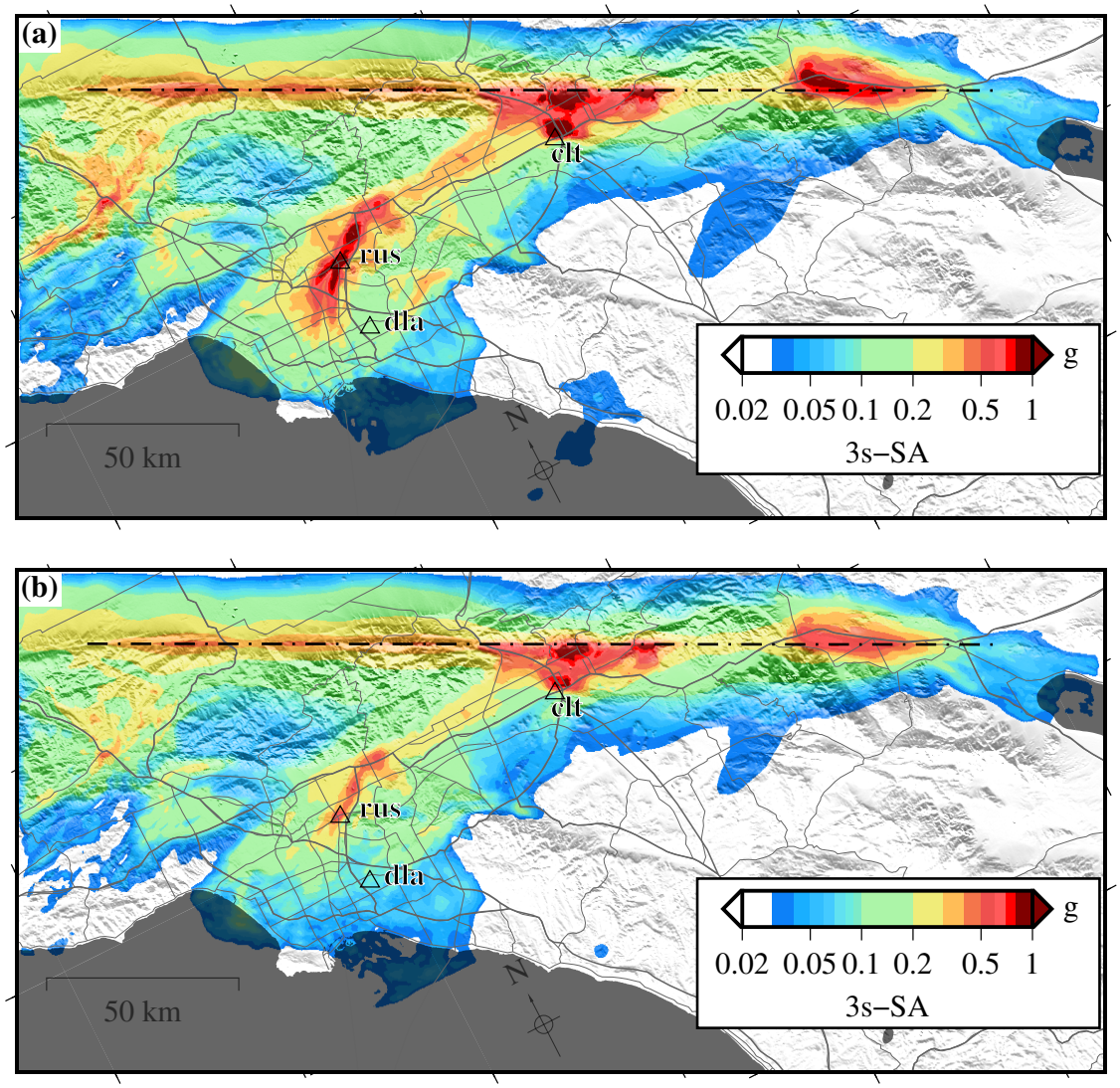

Figure 8: Spectral accelerations at 3s (3s-SAs) obtained in M 7.8 southern San Andreas scenario for (a) a linear medium and (b) a nonlinear medium using the Iwan model. The dashed line shows the fault. Triangles indicate the locations of sites shown in Figure 9.

Code performance

The ShakeOut simulation using AWP-Iwan took 26 hours using 5,600 CPU cores (175 nodes) on NCSA Blue Waters, which represents a 15–20 fold increase with respect to a linear computation. Because the overhead of the Iwan model was larger than the theoretical value of $\sim$10 expected from using 10 yield surfaces, this indicates that the scalability of the code is adversely affected by the large volume of stress tensor data that needs to be exchanged. These difficulties are exacerbated by the shear modulus reduction encountered at large strains, which require nonlinear simulations to be carried out at higher resolution than linear simulations. These performance issues are currently being addressed within in SCEC project 18168 by implementing the

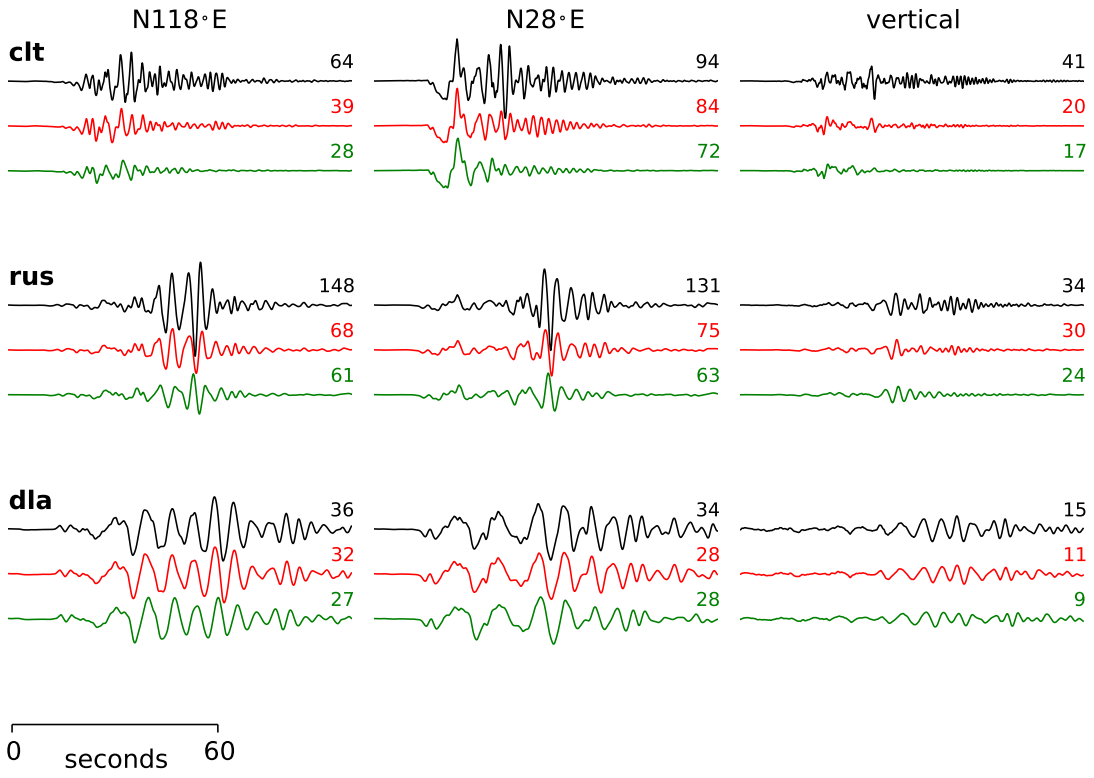

Figure 9: Three-component velocity seismograms obtained for a viscoelastic material (black), a visco-elasto-plastic material using a single Drucker-Prager yield surface (red) and a nonlinear material described by the Iwan model (green). Numbers above each trace denote the peak value in cm/s. See Figure 8 for site locations.

Iwan model in the efficient and scalable GPU version of AWP. Because the GPU code does not depend on swapping stress information (Cui *et al.*, 2013), the Iwan model is not expected to affect scalability of the method. In addition, the GPU code supports discontinuous FD meshes, allowing for high resolution near the surface, where seismic velocities are low and nonlinear effects are most pronounced.

Summary and Outlook

We have successfully implemented the Iwan plasticity model in the CPU version of the AWP finite difference code. The method has been verified against Noah using 1D and 2D site response simulations. AWP-Iwan was deployed on NCSA Blue Waters to simulate a M 7.8 earthquake on the southern San Andreas fault, confirming that nonlinearity will significantly affect the amplitude of long-period surface waves in the LAB during a ShakeOut-type earthquake scenario.

The method is currently being implemented in the scalable and efficient GPU version of AWP. We plan to validate AWP-Iwan against ground motion observations within the PREEVENTS project and to perform more simulations of large southern San Andreas earthquake scenarios for frequencies beyond 1 Hz. We also propose to verify AWP-Iwan against other 3D nonlinear wave propagation codes within the SCEC TAG on shallow crustal effects.

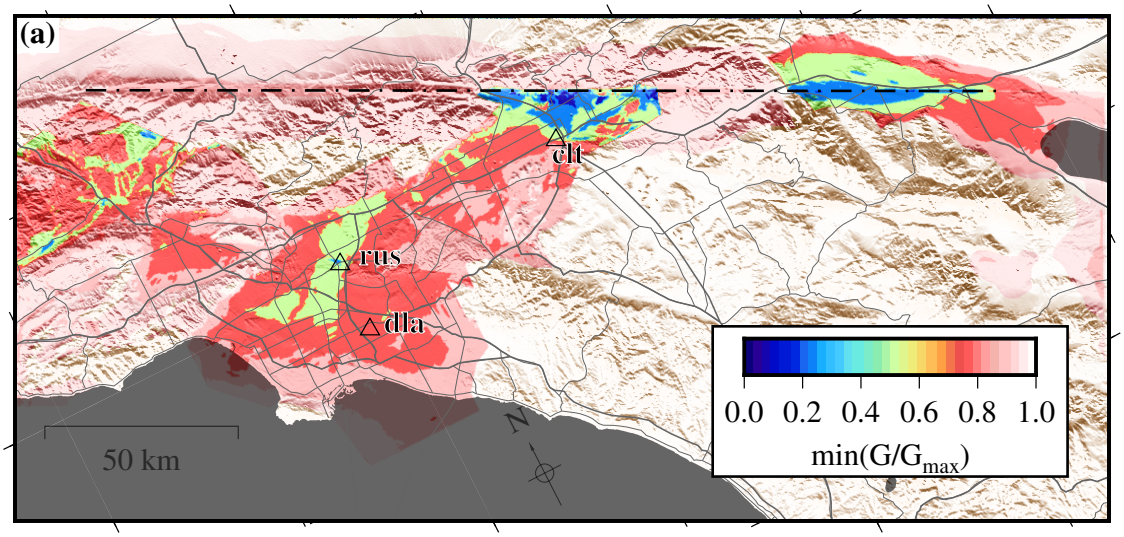

Figure 10: Minimum value of shear modulus G, normalized by low-strain shear modulus $G_{\max}$, at the free surface encountered during the simulation.

Acknowledgements

We thank Fabian Bonilla for providing the Noah codes and for his helpful advice on running the verification simulations. The PIs are grateful to the Southern California Earthquake Center for funding this project. The San Andreas simulations were carried out on NCSA Blue Waters under allocation PRAC_baln.

References

Andrews, D.J. 2005. Rupture dynamics with energy loss outside the slip zone. *J. Geophys. Res*, **110**(B1), B01307.

Bielak, J., Graves, R.W., Olsen, K.B., Taborda, R., Ramírez-Guzmán, L., Day, S.M., Ely, G.P., Roten, D., Jordan, T.H., Maechling, P.J., *et al.* 2010. The ShakeOut earthquake scenario: Verification of three simulation sets. *Geophys. J. Int.*, **180**(1), 375–404.

Bonilla, LF. 2001. NOAH: User's Manual. *Institute for Crustal Studies, University of California, Santa Barbara*.

Bonilla, L.F., Archuleta, R.J., and Lavallee, D. 2005. Hysteretic and Dilatant Behavior of Cohesionless Soils and Their Effects on Nonlinear Site Response: Field Data Observations and Modeling. *Bull. Seism. Soc. Am.*, **95**(6), 2373–2395.

Bonilla, L.F., Luis, P.-C., and Nielsen, S. 2006. 1D and 2D linear and nonlinear site response in the Grenoble area. *In: Third International Symposium on the Effects of Surface Geology on Seismic Motion, Grenoble, France, 30 August - 1 September 2006*. 82.

Chiang, D.-Y. 1992. *Parsimonious modeling of inelastic systems*. Ph.D. thesis, California Institute of Technology.

Chiang, D.Y., and Beck, J.L. 1994. A new class of distributed-element models for cyclic plasticity—I. Theory and application. *International journal of solids and structures*, **31**(4), 469–484.

Cui, Y., Olsen, K.B., Lee, K., Zhou, J., Small, P., Roten, D., Ely, G., Panda, D.K., Chourasia, A, Levesque, J., Day, S.M., and Maechling, P. 2010. Scalable Earthquake Simulation on Petascale Supercomputers. *In: Proceedings of SC10, November 13-19, New Orleans, LA*.

Cui, Y., Poyraz, E., Olsen, K.B., Zhou, J., Withers, K., Callaghan, S., Larkin, J., Guest, C., Choi, D., Chourasia, A., *et al.* 2013. Physics-based seismic hazard analysis on petascale heterogeneous supercomputers. *Page 70 of: Proceedings of the International Conference on High Performance Computing, Networking, Storage and Analysis*. ACM.

Denolle, M.A., Dunham, E.M., Prieto, G., and Beroza, G. 2013. Strong Ground Motion Prediction using Virtual Earthquakes. *Science (2013)*, **343**.

Duan, B., and Day, S.M. 2010. Sensitivity Study of Physical Limits on Ground Motion at Yucca Mountain. *Bull. seism. Soc. Am.*, **100**(6), 2996–3019.

Einav, I. 2005. A second look at strain space plasticity and latest applications. *Pages 225–231 of: Proc. 18th Australian conference on the mechanics of structures and materials (ACMSM). Perth*, vol. 1.

Einav, I., and Collins, I. 2008. A thermomechanical framework of plasticity based on probabilistic micromechanics. *Journal of Mechanics of Materials and Structures*, **3**(5), 867–892.

Electric Power Research Institute. 1993. Guidelines for determining design basis ground motions. *Electric Power Research Institute Technical Report EPRI TR-102293*.

Gélis, C., and Bonilla, L.F. 2012. 2-DP–SV numerical study of soil–source interaction in a non-linear basin. *Geophys. J. Int.*, **191**(3), 1374–1390.

Gélis, C., and Bonilla, L.F. 2014. Influence of a sedimentary basin infilling description on the 2-D P–SV wave propagation using linear and non-linear constitutive models. *Geophys. J. Int.*, **198**(3), 1684–1700.

Graves, R. W., Aagaard, B. T., Hudnut, K. W., Star, L. M., Stewart, J. P., and Jordan, T. H. 2008. Broadband simulations for Mw 7.8 southern San Andreas earthquakes: Ground motion sensitivity to rupture speed. *Geophys. Res. Lett.*, **35**, L22302.

Hardin, B.O., and Drnevich, V.P. 1972. Shear modulus and damping in soils: design equations and curves. *ASCE Journal of Soil Mechanics & Foundations Div*, **98**(sm7), 667–692.

Harris, R. A., Barall, M., Andrews, D.J., Duan, B., Ma, S., Dunham, E.M., Gabriel, A.-A., Kaneko, Y., Kase, Y., Aagaard, B.T., Oglesby, J.-P., Ampuero, J.P., Hanks, T.C., and Abrahamson, N. 2011. Verifying a computational method for predicting extreme ground motion. *Seism. Res. Lett.*, **82**(5), 638–644.

Iai, S., Matsunaga, Y., and Kameoka, T. 1992. Strain space plasticity model for cyclic mobility. *Soils. Found.*, **32**(2), 1–15.

Iwan, W.D. 1967. On a class of models for the yielding behavior of continuous and composite systems. *J. Appl. Mech*, **34**(4), 612–617.

Jones, L. M., Bernknopf, R., Cox, D., Goltz, J., Hudnut, K., Mileti, D., Perry, S., Ponti, D., Porter, K., Reichle, M., Seligson, H., Shoaf, K., Treiman, J., and Wein, A. 2008. *The ShakeOut Scenario*. USGS Open File Report2008-1150. Geological Survey (US).

Joyner, W. B. 2000. Strong Motion from Surface Waves in Deep Sedimentary Basins. *Bull. seism. Soc. Am.*, **90**(6B), S95–112.

Kaklamanos, J., Dorfmann, L., and Baise, L. G. 2015. A Simple Approach to Site-Response Modeling: The Overlay Concept. *Seismological Research Letters*, **86**(2A), 413–423.

Kramer, S. L. 1996. *Geotechnical earthquake engineering*. Prentice Hall, New Jersey.

Ma, S. 2008. A physical model for widespread near-surface and fault zone damage induced by earthquakes. *Geochemistry Geophysics Geosystems*, **9**(11), Q11009.

Masing, G. 1926. Eigenspannungen und Verfestigung beim Messing. *In: Proc. 2nd Int. Congress of Applied Mechanics, Zürich*, vol. 332.

Mroz, Z. 1967. On the description of anisotropic workhardening. *Journal of the Mechanics and Physics of Solids*, **15**(3), 163–175.

Olsen, K. B., Day, S. M., Minster, J. B., Cui, Y., Chourasia, A., Faerman, M., Moore, R., Maechling, P., and Jordan, T. 2006. TeraShake: Strong shaking in Los Angeles expected from southern San Andreas earthquake. *Seism. Res. Lett.*, **77**, 281–282.

Olsen, K. B., Day, S. M., Dalguer, L. A., Mayhew, J., Cui, Y., Zhu, J., Cruz-Atienza, V., Roten, D., Maechling, P., Jordan, T., Okaya, D., and Chourasia, A. 2009. ShakeOut-D: Ground Motion Estimates Using an Ensemble of Large Earthquakes on the Southern San Andreas Fault With Spontaneous Rupture Propagation. *Geophys. Res. Lett.*, **36**, L04303.

Régnier, J., Bonilla, L.F., Bard, P.Y., Kawase, H., Bertrand, E., Hollender, F., Marot, M., Sicilia, D., and Nozu, A. 2015. PRENOLIN Project: a benchmark on numerical simulation of 1D non-linear site effects. 2-Results of the validation phase. *Pages 1–4 of: 6th International conference on earthquake geotechnical engineering*.

Régnier, J., Bonilla, L.F., Bard, P.-Y., Bertrand, E., Hollender, F., Kawase, H., Sicilia, D., Arduino, P., Amorosi, A., Asimaki, D., *et al.* 2018. PRENOLIN: International benchmark on 1D nonlinear site-response analysis—Validation phase exercise. *Bulletin of the Seismological Society of America*, **108**(2), 876–900.

Roten, D., Olsen, K.B., Day, S.M., Cui, Y., and Fäh, D. 2014. Expected seismic shaking in Los Angeles reduced by San Andreas fault zone plasticity. *Geophys. Res. Lett.*, **41**(8), 2769–2777.

Roten, D., Olsen, K.B., Day, S.M., and Cui, Y. 2016. High-Frequency Nonlinear Simulations of Southern San Andreas Earthquake Scenarios. *In: SCEC 2016 Annual Meeting proceeding and abstracts*.

Roten, D., Olsen, K.B., Cui, Y., and Day, S.M. 2017. Quantification of fault zone plasticity effects with spontaneous rupture simulations. *Pure and Applied Geophysics*, 1–23.

Schnabel, P., Seed, H. Bolton, and Lysmer, J. 1972. Modification of seismograph records for effects of local soil conditions. *Bull. Seism. Soc. Am.*, **62**(6), 1649–1664.

Sleep, N. H. 2010. Nonlinear behavior of strong surface waves trapped in sedimentary basins. *Bull. Seism. Soc. Am.*, **100**(2), 826–832.

Sleep, N. H. 2014. Ambient tectonic stress as fragile geological feature. *Geochemistry, Geophysics, Geosystems*, **15**(9), 3628–3644.

Sleep, N. H., and Erickson, B. A. 2014. Nonlinear attenuation of S-waves and Love waves within ambient rock. *Geochemistry, Geophysics, Geosystems*, **15**(4), 1419–1440.